

International Conference on Space Optics—ICSO 2012

Ajaccio, Corse

9–12 October 2012

Edited by Bruno Cugny, Errico Armandillo, and Nikos Karafolas



GAIA Basic Angle Monitoring system

W. Gielesen

D. de Bruijn

T. van den Dool

F. Kamphues

et al.



Testing the LISA optical bench

M. Tröbs*, L. d’Arcio[†], S. Barke*, J. Bogenstahl*, I. Bykov*, M. Dehne*, C. Diekmann*, E. D. Fitzsimons[¶], R. Fleddermann*, O. Gerberding*, J.-S. Hennig*, F. G. Hey[‡], H. Hogenhuis[§], C. J. Killow[¶], E. Kochkina*, J. Kullmann*, M. Lieser*, S. Lucarelli[‡], M. Perreur-Lloyd[¶], J. Pijnenburg[§], D. I. Robertson[¶], A. Shoda*, A. Sohmer[‡], A. Taylor[¶], G. Wanner*, H. Ward[¶], D. Weise[‡], G. Heinzel*, K. Danzmann*

*Albert Einstein Institute, Callinstrasse 38, 30167 Hannover, Germany Email: michael.troeb@aei.mpg.de

[†]ESA/ESTEC, Postbus 299, 2200 AG Noordwijk, The Netherlands

[‡]EADS Astrium GmbH – Satellites, 88039 Friedrichshafen, Germany

[§]TNO Science & Industry, P.O. Box 155, 2600 AD Delft, The Netherlands

[¶]University of Glasgow, Glasgow G12 8QQ, Scotland, UK

Abstract—The Laser Interferometer Space Antenna (LISA) aims to detect gravitational-waves down to mHz frequencies. It will consist of three spacecraft forming an equilateral triangle in an Earth-like orbit around the sun. Drag-free test masses define the arms of a Michelson interferometer that is implemented by mutual laser links between the satellites in a transponder configuration. Each LISA satellite carries optical benches, one for each test mass, that measure the distance variations to the local test mass and to the remote optical bench on the distant satellite. In addition, the optical bench includes an acquisition sensor and mechanisms for laser redundancy switching and point ahead angle correction.

Currently, an elegant bread board of the optical bench is developed and will be characterised. This requires to complete externally the two interferometers mentioned above by simulators - a test mass simulator and a telescope simulator. We will give an overview of the test infrastructure including the overall setup, the simulators, and the phase measurement system.

I. INTRODUCTION

The Laser Interferometer Space Antenna (LISA) [1] aims to detect gravitational waves in the frequency range from 0.1 mHz to 1 Hz. The mission will consist of three satellites that orbit the sun in a heliocentric orbit, following the earth. Each satellite will carry free-flying test masses that define the endpoints of the interferometer arms. Laser light transmitted between the satellites will be used to read out the armlength changes with picometre/ $\sqrt{\text{Hz}}$ accuracy. For this purpose the main optical instrument on the satellite, the optical bench (OB), contains a test mass interferometer that measures the distance between test mass and OB and a so-called science interferometer, that measures the distance between local OB and the OB on the remote satellite. In addition, the OB houses a reference interferometer for the test mass readout and an auxiliary interferometer, that measures pathlength changes by the so-called point ahead angle mechanism (PAAM) [2].

Currently, an elegant breadboard of the LISA OB is in development by a consortium consisting of EADS Astrium GmbH – Satellites as prime contractor to the European Space Agency (ESA), TNO Science & Industry, University of Glasgow and Albert Einstein Institute [3]. Although this project was initiated while LISA was the L1 candidate mission, the basic metrology

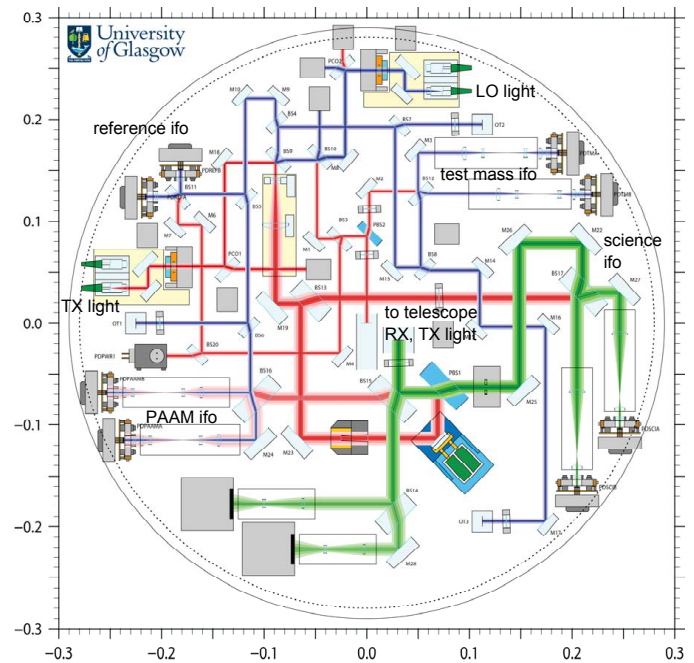


Fig. 1. Layout of the LISA optical bench.

functions implemented and the results are also applicable to NGO/eLISA [4], [5].

Figure 1 shows the layout of the OB. The TX laser injects about 1.6 W of light at 1064 nm wavelength on the left hand side. The main fraction of this light will be sent to the telescope and from there to the distant satellite. A fraction of the light is used for local interferometer readouts and another fraction is transmitted to the second OB on the same satellite. In the same way, light from the other OB on the satellite is injected to the OB on the top in Fig. 1 via the so-called backlink fiber. On the OB this so-called LO light is used with the TX light in the reference, PAAM, and test mass interferometer (in the upper left, lower left, and upper right in the figure, respectively). The science interferometer (in the lower right) interferes light from the distant satellite (RX light) with local TX light. Heterodyne interferometry will be used

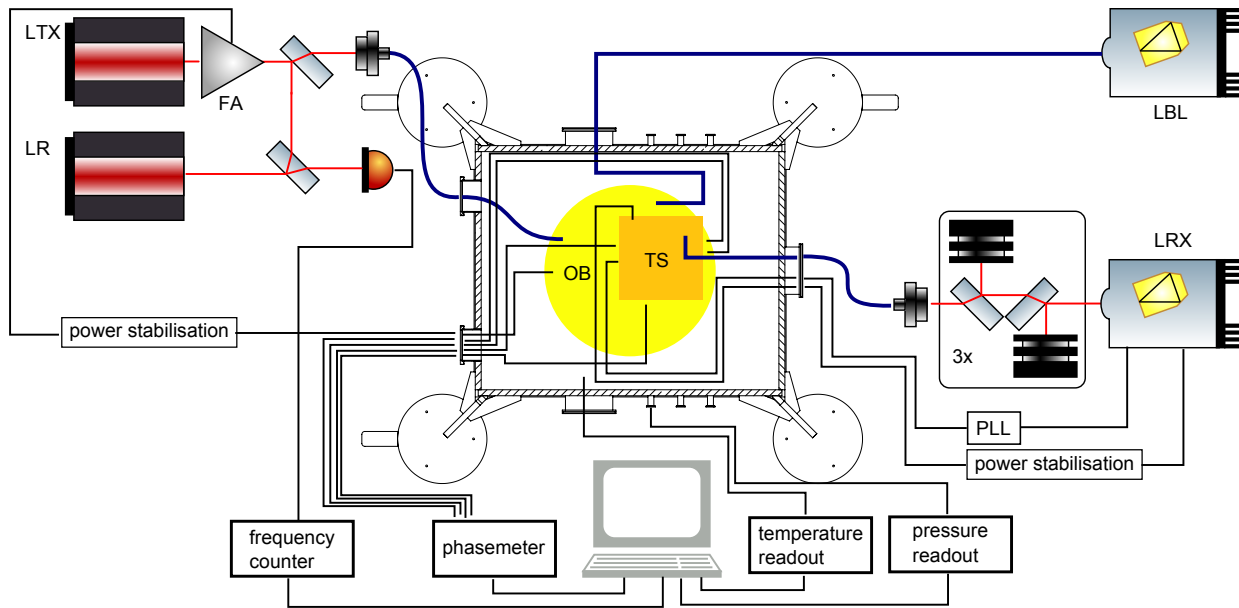


Fig. 2. Schematic layout of the test setup with optical bench, test mass and telescope simulator, lasers, temperature measurement system, and phase measurement system.

with heterodyne frequencies in the range from 2 to 20 MHz.

Characterisation of the OB requires to externally close the test mass interferometer and the science interferometer by simulators and read-out of the respective photo detectors with a phase measurement system. In the following sections we give an overview of the experimental setup, the phase measurement system and the test mass and telescope simulator.

II. EXPERIMENTAL SETUP

Figure 2 shows a simplified schematic of the experimental setup that will be used to test the performance of the science interferometer. Optical bench as well as telescope and test mass simulator will be placed inside the vacuum chamber (the simulator will be placed on top of the optical bench through Zerodur legs for pathlength stability). A combination of scroll pump and turbo pump is connected via diaphragm bellows to the chamber and keeps the pressure at a level below 10^{-5} mbar. The chamber rests on a self-levelling vibration isolation system that is also used for optical tables. It decouples the chamber from vibrations caused by e.g. the vacuum pumps. Laser LTX is a commercial nonplanar ring oscillator laser (Prometheus 20 by Innolight), that generates about 700 mW of output power at 1064 nm and uses a non-linear crystal in single-pass transmission to generate laser light of a few mW at the second harmonic frequency. This green light is used for frequency stabilisation of the laser to molecular iodine using modulation-transfer spectroscopy [6]. The laser output is amplified by an Ytterbium-doped fiber amplifier (PSFA-1064-01-5W-1-3 by Nufern). About 1.6 W of optical power will be injected to the optical bench. Laser LR is an identical frequency stabilised laser system (without amplifier) that is used for frequency noise characterisation. The differential frequency noise between both stabilised lasers is

about $300 \text{ Hz}/\sqrt{\text{Hz}} \times u_{\text{PL}}(f)$ where the shape factor $u_{\text{PL}}(f)$ is given by

$$u_{\text{PL}}(f) = \sqrt{1 + \left(\frac{2.8 \text{ mHz}}{f}\right)^4}.$$

The output of laser LBL is transmitted to the optical bench and is required for operation of reference, test mass and PAAM interferometers. When used, the frequency of laser LBL will be offset-phase-locked to laser LTX to a difference frequency in the 2 to 20 MHz range. For operation of the science interferometer lasers LTX and LRX are required. Laser LRX is then transmitted to the telescope simulator. The signal from the transponder interferometer is used to offset-phase-locked laser LRX to laser LTX. In the beam path of laser LRX up to three mirror pairs can be inserted to attenuate the beam power. Mirror pairs with 45° angle of incidence were chosen because the beam direction and location is not altered upon insertion of the attenuators. A fraction of the power transmitted to optical bench and telescope simulator will be split off and measured with photodetectors. Their signals will be used to stabilise the laser output powers by feeding back to the fiber amplifier pump current and the laser pump current, respectively. The photodetector signals of the interferometers in use will be input to the phase measurement system, also called phasemeter, that is described in Sec. III. As auxiliary data, temperature sensors will be placed at different locations and the pressure in the vacuum chamber and the difference frequency between both stabilised lasers can be recorded.

Figure 3 shows a schematic side view of the vacuum chamber. It will contain the optical bench with the telescope simulator on top. They will be surrounded by a thermal shield. The shield consists of walls of sheet Aluminum on an Aluminum baseplate. The optical bench and the thermal

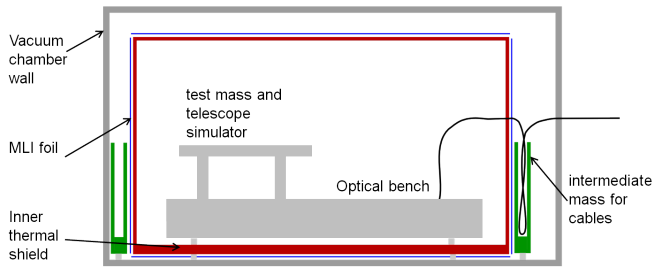


Fig. 3. Schematic of the vacuum chamber with thermal shield.

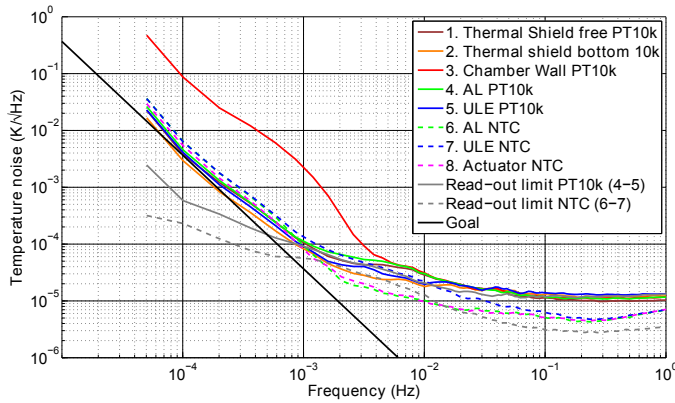


Fig. 4. Temperature noise in the vacuum chamber at different locations.

shield baseplate will rest on ceramic spacers made of Macor. Shield and spacer act as thermal low pass for heat conduction. The shield acts as a thermal capacitor, the spacers as thermal resistors. The metal shield is completely covered by multi-layer insulation (ten pairs of reflecting foil and spacer) to increase the thermal resistance for thermal radiation. The thermal shield is surrounded by an intermediate mass made of Aluminum resting on Macor spacers. All cables connected to optical bench or simulator will be brought into contact with the intermediate mass before they are connected to feedthroughs in the vacuum chamber walls. The intermediate mass reduces temperature fluctuations of the cables originating from the laboratory environment.

Figure 4 shows the temperature noise in the vacuum chamber at different locations. During the temperature noise measurement, the LISA optical bench was replaced by an optical bench that was used for interferometric actuator characterisation. The trace labelled ‘goal’ shows the temperature noise $n_T(f)$ we aim for during LISA optical bench testing, which is given by

$$n_T(f) = 9.1 \cdot 10^{-8} \frac{\text{K}}{\sqrt{\text{Hz}}} \times u_T(f), \quad (1)$$

where $u_T(f)$ is given by

$$u_T(f) = \sqrt{1 + \left(\frac{20 \text{ mHz}}{f}\right)^4}.$$

Two different types of temperature sensors were used: Negative temperature coefficient thermistors (NTCs, dashed lines)

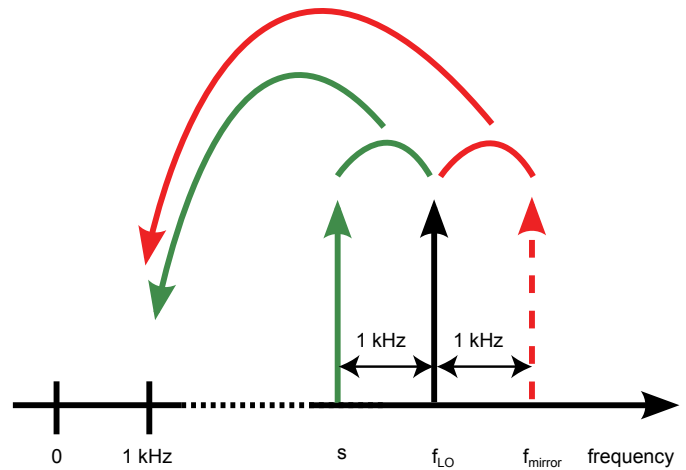


Fig. 5. Mixing of noise to interferometer heterodyne frequency. White noise present at the mirror frequency is folded to the downmixed signal, increasing its noise level by a factor of $\sqrt{2}$.

and platinum sensors (PT, solid lines) both with resistances of 10 k Ω at 25 $^{\circ}\text{C}$. The traces labelled ‘read-out limit’ were generated from the differences of two sensors each. They show the uncorrelated noise between these two channels and are a measure for the sensitivity of the temperature measurement system. With PT and NTC sensors, temperature noise floors of $10^{-5} \text{ K}/\sqrt{\text{Hz}}$ and $3 \cdot 10^{-6} \text{ K}/\sqrt{\text{Hz}}$ were reached, respectively. For frequencies below 1 mHz, the measured temperature noise within the thermal shield was compliant with the goal, for higher frequencies the measurement was sensor-noise limited.

III. PHASE MEASUREMENT SYSTEM

Initially we planned to use the phase measurement system (PMS) of LISA Pathfinder [7] for input signal frequencies in the kHz range. This would have required to mix the heterodyne signals generated on the optical bench from MHz frequencies to kHz frequencies. However, such a downmixing increases the phase readout noise by a factor of $\sqrt{2}$ when an additive white noise floor is present. This is caused by the folding of mirror frequencies, containing noise, to the downmixed signal as is shown in Fig. 5. Although filtering of the mirror frequencies is possible in theory, it is not a practical solution. Figure 6 shows that the phase noise requirement of the science interferometer cannot be met with signal downmixing from MHz to kHz. With downmixing, shot noise, electronic noise and laser power noise completely use the allocated noise, leaving no room for the other noise sources (see discussion in Section IV-E). Instead of the PMS of LISA Pathfinder, a LISA-style MHz tracking PMS will be used of which a prototype became available during the course of this activity. The LISA PMS directly digitises analog signals at MHz frequencies, and tracks their phase via an all-digital phase-locked loop. This allows to measure the signal frequency, phase and amplitude with a high bandwidth [8].

Figure 7 shows the schematic of one channel of the LISA PMS [8]. External to the PMS, two laser beams are interfered and detected by a photodiode. The current of the photodiode

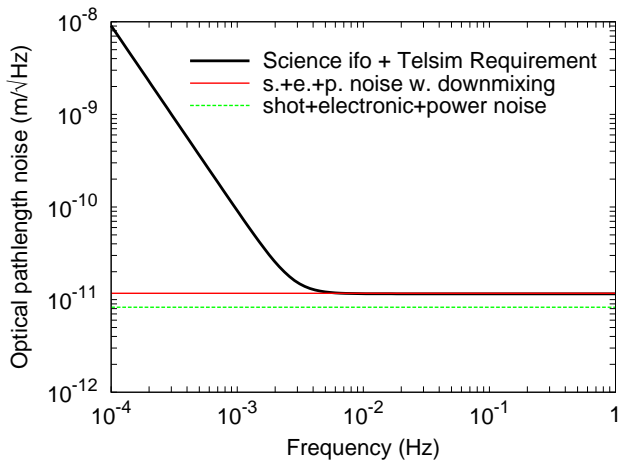


Fig. 6. Effect of downmixing on predicted telescope simulator performance.

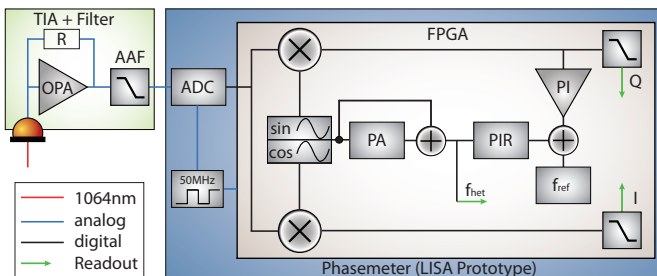


Fig. 7. Schematic of LISA phase measurement system

is converted to a voltage by the transimpedance amplifier (TIA) and filtered by an anti-aliasing filter (AAF) before being digitised by an analog-to-digital converter (ADC). The digital signal is mixed with sine and cosine local oscillator signals of the same frequency. This yields quadrature (Q) and in-phase (I) signals, respectively. The latter is a measure for the amplitude of the heterodyne signal, the former is the phase difference between input signal and local oscillator. This phase difference is used in a control loop to adjust the frequency and phase of the local oscillator signal to the input signal. For this purpose the Q signal is amplified by a proportional-integral amplifier, a constant reference frequency is added and the sum is input to the phase increment register (PIR). The PIR, the phase accumulator (PA), and the lookup table for sine/cosine form a numerically controlled oscillator (NCO). The main outputs of the PMS are the values of the PIR and the PA registers, that correspond to frequency and phase of the input signal, respectively.

A prototype PMS operating as described above has shown sufficient performance for LISA optical bench testing when operated with electrically generated signals. For optical bench testing sixteen analog input channels will be processed by the FPGA.

IV. TEST MASS AND TELESCOPE SIMULATOR

The telescope simulator receives a fraction of TX light emitted from the optical bench and interferes it with light

that is sent to the science interferometer in the so-called transponder interferometer. The latter acts as reference for the science interferometer. In addition to the transponder interferometer, the telescope simulator houses the so-called commissioning interferometer. It can be used to verify the pathlength noise performance of the telescope simulator itself.

A. Purpose and requirements

The test mass simulator should allow optical pathlength noise measurements to verify $2.82 \text{ pm}/\sqrt{\text{Hz}} \times u_{\text{PL}}(f)$ accuracy for a well aligned test mass, which means the returned beam is misaligned to the reference beam by up to $10 \mu\text{rad}$. In addition to that, a working interferometer readout should be demonstrated for misalignments up to $500 \mu\text{rad}$.

The purpose of the telescope simulator is to

- enable optical pathlength measurements of the science interferometer for beam angles within $\pm 10 \mu\text{rad}$ with a measurement noise below $10.5 \text{ pm}/\sqrt{\text{Hz}} \times u_{\text{PL}}(f)$
- enable beam angle measurement noise of less than $12.2 \text{ nrad}/\sqrt{\text{Hz}}$ for beam angles within $\pm 10 \mu\text{rad}$ assuming maximum RX beam tilt jitter of $448 \text{ nrad}/\sqrt{\text{Hz}} \times u_{\text{PL}}(f)$
- provide an RX beam with tilt angles within $\pm 100 \mu\text{rad}$ for functional testing of the science interferometer
- provide an RX beam with tilt angles within $\pm 16 \text{ mrad}$ for testing of the acquisition sensor

We allow for a 10% increase of the requirements by test mass simulator and telescope simulator, respectively.

B. Design considerations

Tilt actuators are required in the telescope simulator for two purposes:

- 1) The RX beam generated by the telescope simulator must be aligned to the TX beam in the science interferometer on the optical bench and
- 2) the light interfering with the TX light on the telescope simulator must be aligned to the TX beam.

For both purposes, four degrees of freedom are required each. This is achieved by using pairs of mirrors on tip-tilt mounts, of which the first one is used to set the reflection point on the second one, which in turn sets the direction of the beam.

In the test mass simulator for the LISA technology package (LTP) it was observed that PZT stacks only fulfill the LTP length noise requirement for low actuation voltages not sufficient for the complete angle range. Hence, we restricted the choice to those commercially available actuators that do not need a voltage applied to them to stay at an arbitrary angle (set-and-forget devices). Here, the AG-M100N-V6 by Newport was chosen as baseline actuator.

The requirements on the RX beam generated by the telescope simulator restrict its power to about 300 pW being detected in the science interferometer. Such small light powers are not detectable by IR-viewer cards commonly used to trace the beam path of IR laser beams. The photo diodes to be used in the science interferometer also exhibit a dark current higher

than the current that would be generated by a beam of this light power, also rendering them useless in alignment of this beam.

These properties of the beam and possible detectors show that no signal can be produced to guide the alignment. The only remaining alternative for alignment is to scan the beam across all possible angles and positions and wait for a “by chance” alignment of the two interfering beams within 500 μ rad to allow for efficient heterodyne detection and the generation of differential wavefront sensing (DWS) alignment signals [9], [10]. Obviously, this would be a lengthy and cumbersome procedure which calls for a better way of aligning the two beams.

One way to achieve a better alignment is to increase beam power during the alignment stage and then reduce light power afterwards with as little change of geometry and alignment of the RX beam as possible. This allows to detect the beam using conventional methods (IR viewer card and DC-current of photodiode) during the alignment phase and to switch over to heterodyne detection and the use of DWS signals enabled through this pre-alignment.

Further information on design and construction of test mass and telescope simulator can be found in [11].

C. Layout

Figure 8 shows the layout of the test mass and telescope simulator. It defines the positions of all optics to be bonded on the Zerodur base plate using hydroxide-catalysis bonding [12] to provide the necessary stability. Due to the adjustable optics the tolerances on these positions are sufficiently loose to enable the use of a template for the positioning during the bonding process which greatly eases and speeds up the building process.

The test mass simulator consists of optical components TMSim1 and Mtm. A pick-up mirror will be placed on the LISA OB between PBS2 and the out-of-plane mirror to send light to mirror TMSim1 that reflects the light to mirror Ttm. The latter uses a reflective gold coating and is placed on a tilt actuator and linear actuator to simulate the test mass. This actuator assembly is described in more detail in Sec. IV-D.

All other components on the Zerodur baseplate belong to the telescope simulator, that is described in the following. The mainly s-polarised output beam from the Fibre Injector Optical Subassembly (FIOS) Telsim in the upper right corner is reflected from polarising beam splitter PBS101 to clean the polarisation. Beam splitter BS101 splits the beam into two equal parts. One part is magnified by lens1 and lens2 to 5 mm diameter and reflected by mirrors M4 and M3 (45° angle of incidence). Beam combiner BS6 reflects 1% of the power towards the out-of-plane mirror Mup that sends the RX beam towards the science interferometer on the optical bench. M4 and M3 are mounted in actuator assemblies described in Section IV-D below. They are used to align the RX beam to the science interferometer. The other part of the beam is reflected by mirrors M101 and M102 (41.5° angle of incidence) and directed to beam combiner BS103. There, the beam from the Telsim FIOS interferes with a fraction of the TX beam from

the optical bench. One percent of the p-polarised TX beam is reflected by BS6, reduced in diameter by lens2 and lens1, transmitted through PBS102 and rotated to s polarisation by half-wave plate HWP1. The interference signals of TX beam and RX beam are detected by photo detectors PD1 and PD2. Mirrors M101 and M102 are used to align the transponder interferometer.

A second FIOS, FIOS com, has been placed in the central upper part. It is used for commissioning of the telescope simulator. Its s-polarised output beam is split by BS104 into two parts. The reflected part propagates towards BS6. For commissioning a mirror and quarter-wave plate will be placed between M3 and BS6, that reflect all light back and rotate its polarisation by 90°, such that it is transmitted through PBS102 and interferes at BS103 with light from FIOS Telsim. The part transmitted through BS104 is interfered at BS106 with light from FIOS Telsim. The interference signals in this commissioning interferometer are detected by photo detectors PD3 and PD4. Polarisation cleaning for the light from FIOS com is performed by PBS102 and PBS105. For commissioning, the beam path between BS102 and BS104 has to be blocked. This will be achieved by insertion of a mirror that reflects the light coming from FIOS Telsim to the space between beam dumps BD1 and BD2 where an additional beam dump will be placed.

A fraction of the power emitted from FIOS Telsim and FIOS com is detected by photo detectors behind BS107 and BS105, respectively, to monitor and or stabilise the output power from the FIOSes.

D. Actuator assemblies

The optical paths on telescope and test mass simulator must be stable to $\text{pm}/\sqrt{\text{Hz}}$ for the temperature noise during measurements ($n_T(f)$, cf (1)). In order to achieve stable mirror positions, the tilt actuators for mirrors M3, M4, M101, and M102, and the tilt and linear actuators for the test mass mirror, Mtm, have been mounted on temperature-compensating brass mounts. Figure 9 shows a side view of the assembly for the test mass simulator. The linear actuator (AG-LS25V6 by Newport) is screwed onto the brass mount. It translates the tilt mount (AG-M100N-V6 by Newport) that is screwed on top of it to the left and right. A steel adapter plate with the mirror attached to it is glued to the front side of the tilt mount (facing to the right in Fig. 9) The assembly has been designed to keep the mirror front surface at the same position when the temperature varies. The brass mount has three spring leaf-shaped feet, that are glued to the telescope simulator baseplate. When the length of the brass mount changes with temperature, the two feet at the position of the mirror (only one if visible in Fig. 9) stay in position. The foot at the back then bends. The distances a, b, c, d and the thermal expansion coefficients of the respective materials have been chosen, such that the mirror surface stays at the same location. More precisely, for given materials and given distances a, c, and d we will adjust the thickness b of the steel adapter plate to fine-tune the thermal expansion coefficient $\frac{ds_{\text{Act}}}{dT}$ of the actuator assembly. We aim to achieve $\frac{ds_{\text{Act}}}{dT} \leq 1 \cdot 10^{-8} \text{ m/K}$.

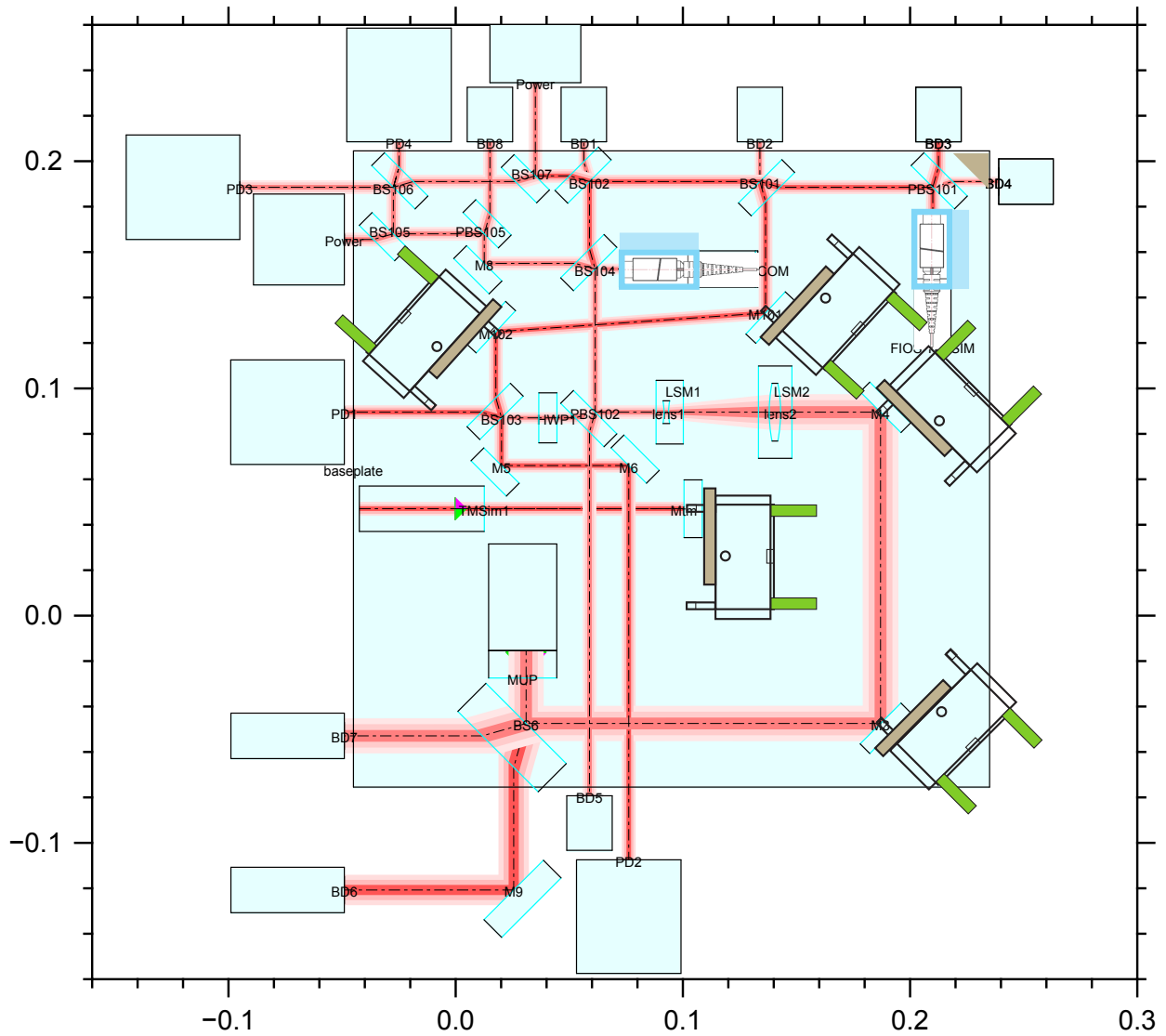


Fig. 8. Schematic layout of test mass and telescope simulator

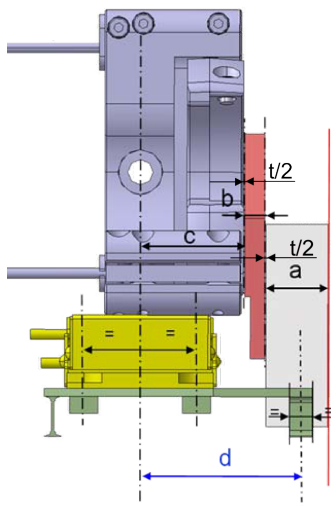


Fig. 9. Side view of actuator assembly

The actuator assemblies for mirrors M101, M102, M3, and M4 use a metal adapter instead of the linear actuator shown in Fig. 9.

E. Performance prediction

In this section we predict the pathlength noise performance of the telescope simulator in combination with the optical bench. We also provide the data required to predict the performance in commissioning mode and of optical bench and telescope simulator individually.

1) *Local noise sources*: First, we consider noise sources that are local to an interferometric readout: shot noise, electronic noise, and relative power noise. They add to the signal at the heterodyne frequency and degrade the interferometric pathlength measurement. Given a signal and a noise of an interferometer readout, its pathlength noise Δs is given by

$$\Delta s = \frac{\lambda \text{ noise}}{2\pi \text{ signal}} \quad (2)$$

where λ is the laser wavelength. We consider the signal and the noise from both ports of the interferometer, i.e. from the combined signals of two quadrant photodiodes with four segments each. The rms signal of the combined photocurrents (in A) is given by

$$\text{signal} = \eta\sqrt{2\gamma P_{\text{sig}} P_{\text{lo}}} \quad (3)$$

where η is the efficiency of the photodiodes, γ the mode overlap (heterodyne efficiency) of the interfering beams and P_{sig} and P_{lo} are the signal and local oscillator power before the recombination beamsplitter, respectively. The shot noise, electronic noise, and relative power noise of the combined photocurrents in ($A/\sqrt{\text{Hz}}$) are given by

$$\text{noise}_{\text{shot}} = \sqrt{2q_e\eta(P_{\text{sig}} + P_{\text{lo}})} \quad (4)$$

$$\text{noise}_{\text{el}} = \sqrt{8n_{\text{el}}} \quad (5)$$

$$\text{noise}_{\text{RPN}} = n_{\text{RPN}}\eta(P_{\text{sig}} + P_{\text{lo}}), \quad (6)$$

where q_e is the elementary charge, n_{el} is the electronic noise per QPD segment, and n_{RPN} is the relative power noise of signal and local oscillator beam. We use $n_{\text{el}} = 3.5 \text{ pA}/\sqrt{\text{Hz}}$ and $n_{\text{RPN}} = 2 \cdot 10^{-8}/\sqrt{\text{Hz}}$ in the following.

Inserting (3) and (4), (5), (6) into (2) yields the pathlength noise due to shot noise, electronic noise and relative power noise for interferometer I .

$$\Delta s_{\text{shot}}(I) = \frac{\lambda}{2\pi} \sqrt{\frac{q_e(P_{\text{sig}}(I) + P_{\text{lo}}(I))}{\eta\gamma P_{\text{sig}}(I)P_{\text{lo}}(I)}} \quad (7)$$

$$\Delta s_{\text{el}}(I) = \frac{\lambda}{\pi} \frac{n_{\text{el}}}{\eta\sqrt{\gamma P_{\text{sig}}(I)P_{\text{lo}}(I)}}, \quad (8)$$

$$\Delta s_{\text{RPN}}(I) = \frac{\lambda}{2\pi} \frac{n_{\text{RPN}}(P_{\text{sig}}(I) + P_{\text{lo}}(I))}{\sqrt{2\gamma P_{\text{lo}}(I)P_{\text{sig}}(I)}}, \quad (9)$$

These three noise sources are independent and hence add quadratically. Their combined pathlength noise $\Delta s_{\text{L}}(I)$ is given by

$$\Delta s_{\text{L}}(I) = \sqrt{\Delta s_{\text{shot}}(I)^2 + \Delta s_{\text{el}}(I)^2 + \Delta s_{\text{RPN}}(I)^2}. \quad (10)$$

The optical powers of signal beam and local oscillator beam are listed in Table I. Tables II and III summarise the parameters and constants used in this and the following sections.

We include a further source of pathlength noise that is caused by the point ahead angle mechanism (PAAM) [2] on the optical bench. Optical pathlength noise generated by the PAAM is required to be below Δs_{PAAM} .

$$\Delta s_{\text{PAAM}} = 1.42 \text{ pm}/\sqrt{\text{Hz}} \quad (11)$$

This requirement has been verified experimentally [2].

2) *Temperature-related local noise sources:* The selected actuators show a coupling from temperature to angle. When reflection point and rotation point do not coincide, the distance l between the two (in a single actuator axis) transforms temperature driven tilts into optical pathlength changes. This pathlength noise Δs_{rot} for a single actuator axis is given by

$$\Delta s_{\text{rot}} = \Delta T \frac{d\phi}{dT} l \cdot 2 \cos \phi,$$

TABLE I
TOTAL OPTICAL POWERS BEFORE RECOMBINATION BEAMSPLITTERS

Interferometer	P_{lo} (W)	P_{sig} (W)
Commissioning	$3.5 \cdot 10^{-3}$	$40.7 \cdot 10^{-9}$
Transponder	$3.9 \cdot 10^{-3}$	$16.3 \cdot 10^{-6}$
PAAM	$1.24 \cdot 10^{-3}$	$0.27 \cdot 10^{-3}$
Reference	$1.33 \cdot 10^{-3}$	$0.88 \cdot 10^{-3}$
Science	$0.27 \cdot 10^{-3}$	$295.5 \cdot 10^{-12}$
Test mass	$0.73 \cdot 10^{-3}$	$20.6 \cdot 10^{-6}$

TABLE II
QUANTITIES USED FOR PERFORMANCE PREDICTION.

Quantity	Symbol	Unit
Actuator angle of incidence	ϕ	rad
Distance between reflection and rotation point	d	m
Thermal expansion of actuator assembly	$\frac{ds_{\text{Act}}}{dT}$	m/K
Pathlength noise of single actuator axis	Δs_{Act}	m/ $\sqrt{\text{Hz}}$
Pathlength noise of all actuators	$\Delta s_{\text{Act,all}}$	m/ $\sqrt{\text{Hz}}$
Pathlength noise due to electronic noise	Δs_{el}	m/ $\sqrt{\text{Hz}}$
Pathlength noise due to frequency noise	Δs_{freq}	m/ $\sqrt{\text{Hz}}$
Pathlength noise of PAAM	Δs_{PAAM}	m/ $\sqrt{\text{Hz}}$
Pathlength noise for single actuator axis	Δs_{rot}	m/ $\sqrt{\text{Hz}}$
Pathlength noise for all actuator rotations	$\Delta s_{\text{rot,all}}$	m/ $\sqrt{\text{Hz}}$
Pathlength noise due to relative power noise	$\Delta s_{\text{RPN}}(I)$	m/ $\sqrt{\text{Hz}}$
Pathlength noise due to shot noise	$\Delta s_{\text{shot}}(I)$	m/ $\sqrt{\text{Hz}}$
Pathlength noise of interferometer I	$\Delta s_{\text{L}}(I)$	m/ $\sqrt{\text{Hz}}$
Pathlength noise of telescope simulator	Δs_{TS}	m/ $\sqrt{\text{Hz}}$
Thermo-elastic noise in fused silica	Δs_{FS}	m/ $\sqrt{\text{Hz}}$
Thermo-elastic noise in Zerodur	Δs_{Z}	m/ $\sqrt{\text{Hz}}$
Optical path difference in fused silica	OPD _{FS}	m
Optical path difference on Zerodur	OPD _Z	m
Local oscillator power	P_{lo}	W
Signal power	P_{sig}	W
Temperature noise	ΔT	K/ $\sqrt{\text{Hz}}$

TABLE III
CONSTANTS AND PARAMETERS USED FOR PERFORMANCE PREDICTION;
COEFFICIENT OF THERMAL EXPANSION CTE, FUSED SILICA FS

Quantity	Symbol	Value	Unit
Speed of light	c	299792458	m/s
Elementary charge	q_e	$1.6 \cdot 10^{-19}$	As
CTE of fused silica	α_{FS}	$5.5 \cdot 10^{-7}$	1/K
CTE of Zerodur	α_{Z}	$2 \cdot 10^{-8}$	1/K
Electr. noise per QPD segment	n_{el}	$3.5 \cdot 10^{-12}$	A/ $\sqrt{\text{Hz}}$
Thermo-optic coeff. of FS	$\frac{dn_{\text{FS}}}{dT}$	$1.1 \cdot 10^{-5}$	1/K
Temp. coeff. of actuator angle	$\frac{d\phi}{dT}$	$4 \cdot 10^{-6}$	rad/K
Therm. exp. of act. ass.	$\frac{ds_{\text{Act}}}{dT}$	10^{-8}	m/K
Photodiode efficiency	η	0.55	1
Heterodyne efficiency	γ	0.8	1
Laser wavelength	λ	1064	nm
Laser frequency noise	Δf	300	Hz/ $\sqrt{\text{Hz}}$
Actuator lever arm	l	2	mm
Refractive index of FS	n_{FS}	1.44963	1
Relative power noise	n_{RPN}	$2 \cdot 10^{-8}$	1/ $\sqrt{\text{Hz}}$

where ϕ is the angle of incidence and $\frac{d\phi}{dT}$ is the angle change per temperature change. The derivation of the factor $2 \cos \phi$ can be found in [13, pp. 102]. This coupling from temperature to pathlength in the tilt actuator requires to minimise the leverarm l , when the pathlength noise of the test mass interferometer is to be characterised. This will be achieved by replacing the linear actuator by a metal adapter of lower height. We assume that we can keep $l \leq 2$ mm both in the test mass simulator as well as in the actuators in the telescope simulator.

Optical pathlength noise due to thermal expansion of the actuator assemblies Δs_{Act} is given by

$$\Delta s_{Act} = \Delta T \frac{ds_{Act}}{dT} \cdot 2 \cos \phi,$$

where $\frac{ds_{Act}}{dT}$ is the expansion coefficient of the actuator assemblies.

3) *Noise sources coupled to two interferometers:* Some noise sources couple via a path imbalance in the length measurement. Interferometric testing of the LISA optical bench requires to read out two interferometers simultaneously. In this case, the coupling factor is given by a length difference between the two interferometers. In this section we discuss the relevant length differences and allocate them to either optical bench or telescope simulator. We quantify the influence of laser frequency noise, thermal expansion of the setup (thermo-elastic noise) and temperature-driven pathlength changes in fused silica (thermo-optic noise) on the length measurement.

Optical pathlength noise due to thermo-optical noise within fused silica Δs_{FS} is given by

$$\Delta s_{FS} = \left| \Delta T \cdot OPD_{FS} \cdot \alpha_{FS} (n_{FS} - 1) + \frac{dn_{FS}}{dT} \right| \quad (12)$$

where ΔT is the temperature noise, OPD_{FS} the effective imbalance in fused silica, α_{FS} the coefficient of thermal expansion of fused silica, n_{FS} its refractive index, and $\frac{dn_{FS}}{dT}$ the change in refractive index with temperature. The -1 in (12) takes into account, that although a temperature increase increases the geometrical path through fused silica (for a positive α_{FS}) but at the same time decreases the pathlength in vacuum.

Optical pathlength noise due to thermo-elastic noise of Zerodur Δs_Z is given by

$$\Delta s_Z = |\Delta T (OPD_Z - OPD_{FS} \cdot \alpha_{FS}) \alpha_Z|, \quad (13)$$

where OPD_Z and α_Z are the path imbalance and coefficient of thermal expansion of Zerodur.

Optical pathlength noise due to laser frequency noise Δs_{freq} is given by

$$\Delta s_{freq} = \left| \frac{\lambda}{c} \cdot OPD_Z \cdot \Delta f \right|, \quad (14)$$

where c is the speed of light and Δf is the laser frequency noise. Figure 10 shows a schematic view on optical bench and telescope simulator. The TX laser is input to the optical bench, the RX laser is input to the telescope simulator. On the optical bench the science interferometer is shown (BS17), on the telescope simulator the transponder interferometer is shown

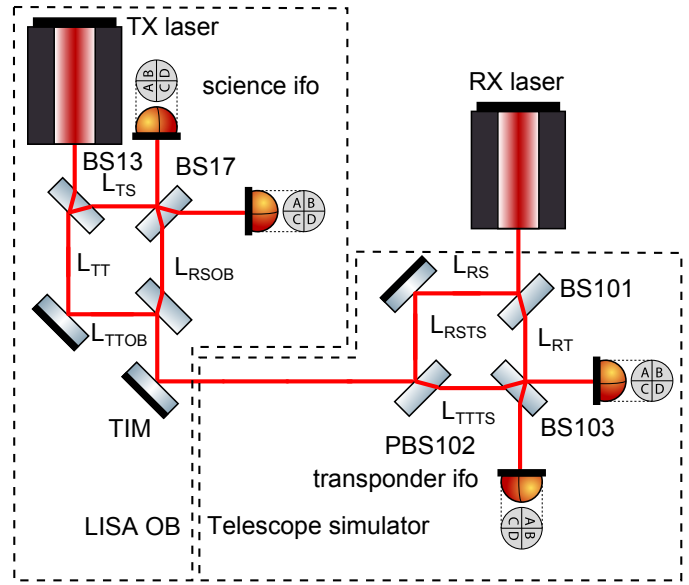


Fig. 10. Schematic view of optical bench and telescope simulator for noise partitioning.

TABLE IV
PATHLENGTH IMBALANCES AND THEIR ENDPOINTS; CF. FIG. 10

Distance	Endpoints
L_{TS}	BS13, BS17
L_{TT}	BS13, BS103
L_{TTOB}	BS13, TIM
L_{TTTS}	TIM, BS103
L_{RT}	BS101, BS103
L_{RS}	BS101, BS17
L_{RSTS}	BS101, TIM
L_{RSOB}	TIM, BS17

(BS103). We define path imbalances ΔL_S and ΔL_T between TX and RX laser in science and transponder interferometer, respectively.

$$\Delta L_S = L_{TS} - L_{RS} \quad (15)$$

$$\Delta L_T = L_{TT} - L_{RT} \quad (16)$$

Table IV lists the endpoints of L_{TS} , L_{RS} , L_{TT} and L_{RT} and all other lengths to be used in this section.

We do not consider the lengths between TX laser and BS13 and RX laser and BS101 because they are common to science and transponder interferometer and hence cancel in the difference of the two. For measurements utilising science and transponder interferometer, the effective length imbalance ΔL is given by

$$\Delta L = \Delta L_S - \Delta L_T. \quad (17)$$

By inserting (15), (16), (18) and (19) into (17)

$$L_{RS} = L_{RSOB} + L_{RSTS} \quad (18)$$

$$L_{TT} = L_{TTOB} + L_{TTTS} \quad (19)$$

we find

$$\Delta L = \Delta L_{OB} + \Delta L_{TS}, \quad (20)$$

TABLE V
EFFECTIVE PATH MISMATCH ON ZERODUR AND IN FUSED SILICA;
OPTICAL BENCH OB, TELESCOPE SIMULATOR TS, TRANSPONDER MODE
TRANSP., COMMISSIONING MODE COMM.

	OPD _Z (mm)	OPD _{FS} (mm)
OB	-564.6	-29.1
TS transp.	-1040.4	-20.3
OB+TS transp.	-1605.1	-49.4
TS comm.	665.1	33.6

with

$$\Delta L_{OB} = L_{TS} - L_{RSOB} - L_{TTOB} \quad (21)$$

$$\Delta L_{TS} = L_{RT} - L_{RSTS} - L_{TTTS}. \quad (22)$$

We have partitioned the effective path imbalance ΔL into a part on the optical bench (ΔL_{OB}) and a part on the telescope simulator (ΔL_{TS}). This scheme was used to produce the effective path imbalances on Zerodur and in fused silica as listed in Table V.

4) *Combinations of noise sources:* In this section we combine the individual noise sources discussed in the previous sections. We assume, all actuator assemblies are identical and exhibit the same temperature noise. Then their pathlength noises add linearly. In the horizontal axis the pathlength noises of M101 and M102 and M3 and M4 cancel each other. In the vertical axis the noises add up:

$$\Delta s_{rot,all} = \Delta T \frac{d\phi}{dT} l \cdot 2 (2 \cos 41.5^\circ - 2 \cos 45^\circ - 2 \cos 45^\circ) \quad (23)$$

The factor of two outside the round brackets in (23) takes two actuators each into account.

The same is true for the combined effect of longitudinal actuator noise with temperature on the optical pathlength noise $\Delta s_{Act,all}$:

$$\Delta s_{Act,all} = \Delta T \frac{ds_{Act}}{dT} \cdot 2 (2 \cos 41.5^\circ - 2 \cos 45^\circ - 2 \cos 45^\circ) \quad (24)$$

Now we combine the noise sources discussed previously. Optical pathlength noise associated with the telescope simulator Δs_{TS} is given by

$$\Delta s_{TS} = \left[(\Delta s_{rot,all} + \Delta s_{Act,all} + \Delta s_Z + \Delta s_{FS})^2 + \Delta s_L(T) + \Delta s_{PAAM}^2 + \Delta s_{freq}^2 \right]^{1/2}. \quad (25)$$

Depending on what path imbalance data from Table V is used, both the pathlength noise performance of the telescope simulator in transponder mode or in commissioning mode can be predicted.

The noise attributed to the optical bench Δs_{OB} is given by

$$\Delta s_{OB} = \sqrt{(\Delta s_Z + \Delta s_{FS})^2 + \Delta s_L(S) + \Delta s_{freq}^2}. \quad (26)$$

Finally, we combine the noise sources of optical bench and telescope simulator and obtain

$$\Delta s_{OB+TS} = \left[(\Delta s_{rot,all} + \Delta s_{Act,all} + \Delta s_Z + \Delta s_{FS})^2 + \Delta s_L(S) + \Delta s_L(T) + \Delta s_{PAAM}^2 + \Delta s_{freq}^2 \right]^{1/2} \quad (27)$$

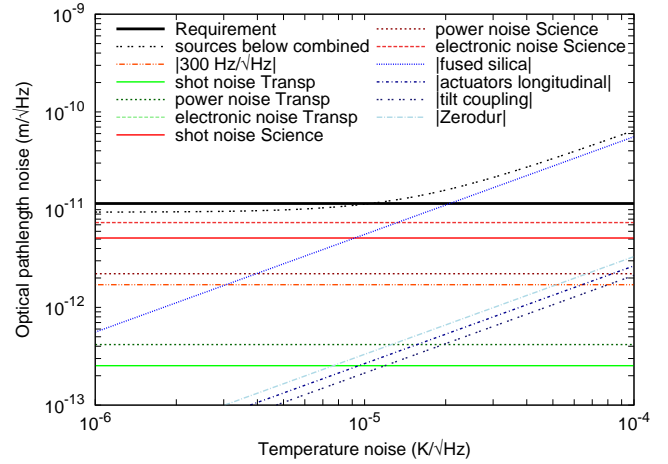


Fig. 11. Performance prediction for optical bench and telescope simulator as function of temperature noise.

for the noise of optical bench and the telescope simulator in transponder mode Δs_{OB+TS} .

Figure 11 shows this predicted pathlength noise performance over temperature noise. For temperature noise below $10^{-5} \text{ K}/\sqrt{\text{Hz}}$ the combined noise is below the requirement. For higher temperature noise thermo-optic noise in fused silica is the dominant noise source followed by electronic noise and shot noise in the science interferometer.

5) *Frequency dependencies:* In Fig. 11 we have considered pathlength noise as function of temperature noise. Now we fix the temperature noise to a specific value and look at the frequency dependencies of the noise contributions.

Pathlength noise due to electronic noise, relative power noise and shot noise has a uniform frequency distribution. We can use (8), (9), (7), and (10) for a fixed temperature noise without modification.

For the local temperature-dependent noise sources tilt coupling Δs_{rot} and thermal expansion Δs_{Act} of actuator assemblies we define an additional noise shape $u_M(f)$

$$u_M(f) = \sqrt{1 + \left(\frac{2 \text{ mHz}}{f} \right)^4}$$

that we multiply with (23) and (24). We use a temperature noise of $10^{-5} \text{ K}/\sqrt{\text{Hz}}$ as approximation to the measured temperature noise shapes shown in Fig. 4.

For the pathlength noise due to the PAAM, Δs_{PAAM} , and frequency noise induced pathlength noise, Δs_{freq} , we multiply (11) and (14) with the shape factor $u_{PL}(f)$.

For pathlength noise on Zerodur, Δs_Z , and pathlength noise in fused silica, Δs_{FS} , (13) and (12) are multiplied with $u_M(f)$.

Figure 12 shows the resulting predicted pathlength noise as function of frequency for $10^{-5} \text{ K}/\sqrt{\text{Hz}} \times u_M(f)$ temperature noise. Since we have demonstrated such temperature noise in the environment foreseen for LISA optical bench testing it seems possible to verify pathlength noise performance of the science interferometer within requirements. At about 3 mHz

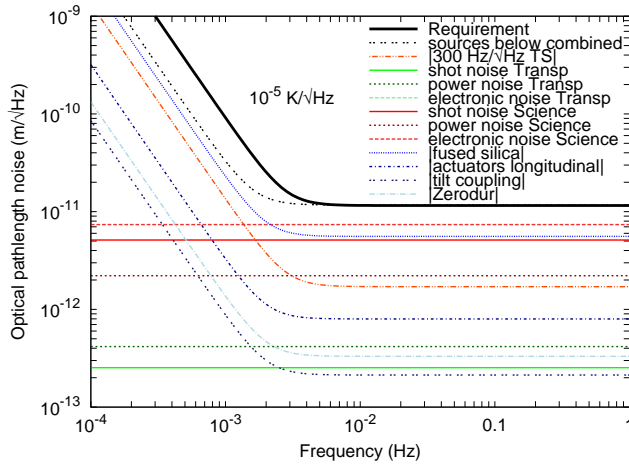


Fig. 12. Performance prediction for optical bench and telescope simulator as function frequency for $10^{-5} \text{ K}/\sqrt{\text{Hz}}$ temperature noise.

the pathlength noise might be slightly higher, depending on the temperature noise during the measurements.

V. CONCLUSION

Testing of the LISA optical bench elegant breadboard requires to externally complete the test mass and science interferometers by simulators. We have presented such simulators that will be implemented on a common Zerodur baseplate. The test mass simulator consists of a gold-coated mirror on a tilt and linear actuator. The telescope simulator works as a transponder and provides a reference for the science interferometer on the LISA OB. Both simulators employ tilt actuators for beam alignment that are held in thermally compensating mounts. The pathlength noise performance of the telescope simulator can be verified independently from the LISA OB by means of a dedicated interferometer on the simulator. In the experiments, temperature noise control will be crucial. On the basis of the measured temperature noise and the performance predictions presented above characterisation of the LISA optical bench to its requirements seems possible.

A tracking phasemeter implemented in a field-programmable gate array (FPGA) will be used as phase measurement system. Prototypes of this phasemeter have shown the required phase noise performance using electrical signals. A 16 channel version of the phasemeter will be used, sufficient to read out two fully redundant interferometers equipped with quadrant photo detectors.

ACKNOWLEDGMENT

We acknowledge funding by the European Space Agency within the project “Optical Bench Development for LISA”, support from STFC and UKSA, and support by Deutsches Zentrum für Luft und Raumfahrt (DLR) with funding from the Bundesministerium für Wirtschaft und Technologie (DLR project reference 50 OQ 0601). We thank the German Research Foundation for funding the cluster of Excellence QUEST - Centre for Quantum Engineering and Space-Time Research.

REFERENCES

- [1] O. Jennrich, “LISA technology and instrumentation,” *Class. Quantum Grav.*, vol. 26, no. 15, AUG 7 2009.
- [2] N. R. J.A.C.M. Pijenburg, “Picometer stable scan mechanism for gravitational wave detection in space: LISA PAAM,” in *Proc. of the International Conference on Space Optics*, 2010.
- [3] L. d’Arcio, J. Bogenstahl, M. Dehne, C. Diekmann, E. D. Fitzsimons, R. Fleddermann, E. Granova, G. Heinzel, H. Hogenhuis, C. J. Killow, M. Perreur-Lloyd, J. Pijenburg, D. I. Robertson, A. Shoda, A. Sohmer, A. Taylor, M. Tröbs, G. Wanner, H. Ward, and D. Weise, “OPTICAL BENCH DEVELOPMENT FOR LISA,” in *Proc. of the International Conference on Space Optics*, 2010.
- [4] “LISA Assessment Study Report,” ESA document ESA/SRE (2011)3, 2011.
- [5] “NGO Assessment Study Report,” ESA document ESA/SRE (2011)19, 2012.
- [6] J. H. Shirley, “Modulation transfer processes in optical heterodyne saturation spectroscopy,” *Opt. Lett.*, vol. 7, no. 11, pp. 537–539, Nov 1982. [Online]. Available: <http://ol.osa.org/abstract.cfm?URI=ol-7-11-537>
- [7] G. Heinzel, V. Wand, A. Garcia, O. Jennrich, C. Braxmaier, D. Robertson, K. Middleton, D. Hoyland, A. Rüdiger, R. Schilling, U. Johann, and K. Danzmann, “The LTP interferometer and phasemeter,” *Class. Quantum Grav.*, vol. 21, pp. S581–S587, 2004.
- [8] I. Bykov, J. J. E. Delgado, A. F. G. Marin, G. Heinzel, and K. Danzmann, “LISA phasemeter development: Advanced prototyping,” *Journal of Physics: Conference Series*, vol. 154, no. 1, p. 012017, 2009. [Online]. Available: <http://stacks.iop.org/1742-6596/154/i=1/a=012017>
- [9] E. Morrison, B. J. Meers, D. I. Robertson, and H. Ward, “Automatic alignment of optical interferometers,” *Appl. Opt.*, vol. 33, pp. 5041–5049, 1994.
- [10] —, “Experimental demonstration of an automatic alignment system for optical interferometers,” *Appl. Opt.*, vol. 33, pp. 5037–5040, 1994.
- [11] J. Bogenstahl, M. Tröbs, L. d’Arcio, C. Diekmann, E. D. Fitzsimons, J.-S. Hennig, F. G. Hey, C. J. Killow, M. Lieser, S. Lucarelli, M. Perreur-Lloyd, J. Pijenburg, D. I. Robertson, A. Taylor, H. Ward, D. Weise, G. Heinzel, and K. Danzmann, “Design and construction of a telescope simulator for LISA optical bench testing,” in *Proc. of the International Conference on Space Optics*, 2012.
- [12] E. J. Elliffe, J. Bogenstahl, A. Deshpande, J. Hough, C. Killow, S. Reid, D. Robertson, S. Rowan, H. Ward, and G. Cagnoli, “Hydroxide-catalysis bonding for stable optical systems for space,” *Classical and Quantum Gravity*, vol. 22, no. 10, p. S257, 2005. [Online]. Available: <http://stacks.iop.org/0264-9381/22/i=10/a=018>
- [13] F. Guzmán Cervantes, “Gravitational wave observation from space: Optical measurement techniques for LISA and LISA Pathfinder,” Ph.D. dissertation, Leibniz Universität Hannover, 2009.